RSC Advances

PAPER

View Article Online
View Journal | View Issue

Cite this: *RSC Adv.*, 2025, **15**, 41710

Bio-dye-sensitized TiO_2 nanophotocatalysts for visible-light-driven sustainable wastewater treatment

Md. Abul Bashar,[a] Ahmed B. M. Ibrahim,[b] Md. Kamrul Hasan [a] and Muhammad Sarwar Hossain *[a]

The limited visible-light activity of titanium dioxide (TiO_2) restricts its application in solar-driven photocatalysis for wastewater treatment. In this study, TiO_2 nanoparticles were sensitized with natural plant-derived dyes-chlorophyll from *Eichhornia crassipes* (water hyacinth) and anthocyanin from *Nymphaea rubra* (red water lily)-to extend their optical response into the visible spectrum. Dye extraction was followed by TiO_2 sensitization, and the resulting nanocomposites were comprehensively characterized using FTIR, UV-Vis, XRD, SEM-EDX, and TGA analyses. Results confirmed successful dye adsorption without altering TiO_2's anatase-dominant crystalline phase. UV-Vis spectra revealed broadened visible-light absorption, particularly in anthocyanin-sensitized TiO_2, due to strong $\pi \rightarrow \pi^*$ transitions and hydroxyl-functional group interactions. Photocatalytic activity was evaluated *via* methylene blue (MB) degradation under visible light, optimizing parameters such as dye concentration, pH, catalyst dosage, and initial pollutant load. Anthocyanin-sensitized TiO_2 exhibited superior performance, achieving 75% degradation under optimal conditions, compared to 66% for chlorophyll-sensitized TiO_2. Neutral pH and moderate catalyst dosage (0.2 g L^{-1}) favored maximum efficiency. Reusability tests over five consecutive cycles demonstrated both catalysts retained over 80% of their initial activity, with anthocyanin-sensitized TiO_2 showing higher stability. This eco-friendly approach leverages abundant, renewable plant pigments to enhance TiO_2's photocatalytic efficiency without costly or hazardous modifications. The findings highlight the potential of natural dye-sensitized TiO_2 as a sustainable and cost-effective photocatalyst for visible-light-driven wastewater treatment, offering a promising pathway toward scalable, green water purification technologies.

Received 19th August 2025
Accepted 17th October 2025

DOI: 10.1039/d5ra06120b

rsc.li/rsc-advances

1. Introduction

Water is one of the most essential resources for sustaining life, ecosystems, and economic activities. However, increasing pressures from industrial growth, urbanization, population expansion, and climate change have drastically reduced both the availability and quality of clean water.[1] Globally, about two billion people lack access to safe drinking water, and approximately five million die each year from diseases caused by contaminated water, highlighting an urgent global health crisis.[2] A significant contributor to water pollution is industrial wastewater, particularly from sectors like textiles, pharmaceuticals, chemicals, food processing, and paper manufacturing. These industries discharge persistent organic pollutants (POPs) that are difficult to remove using traditional treatment methods.[3] The textile industry is among the worst offenders, contributing 17–20% of global industrial water pollution, with 10–15% of dyes used in manufacturing ending up directly in wastewater due to poor fiber binding. Synthetic dyes are notably hard to degrade due to their complex structures and chemical stability. Conventional treatments such as filtration or biological degradation are often ineffective against such contaminants.[4] This has prompted the development of advanced oxidation processes (AOPs), which utilize reactive species like hydroxyl and superoxide radicals to break down pollutants more effectively.[5] AOPs are a class of water treatment methods that rely on the *in situ* generation of powerful oxidants, especially hydroxyl radicals, to mineralize organic contaminants into harmless end products like CO_2 and H_2O.[6,7] Unlike conventional methods that transfer pollutants between phases or generate hazardous by-products, AOPs enable complete degradation without secondary contamination. Among these, photocatalysis is a widely studied AOP due to its ability to harness light energy, especially in the presence of semiconductor materials, to activate oxidation–reduction reactions.[8]

Photocatalytic degradation involves the excitation of a photocatalyst, such as a semiconductor oxide, under light exposure,

[a]*Chemistry Discipline, Khulna University, Khulna-9208, Bangladesh. E-mail: sarwar@chem.ku.ac.bd*

[b]*Department of Chemistry, College of Science, Imam Mohammad Ibn Saud Islamic University (IMSIU), Riyadh 11623, Saudi Arabia*

resulting in the formation of electron–hole pairs that interact with water and oxygen to produce reactive oxygen species (ROS).[9] Common semiconductors used for photocatalysis include TiO_2, ZnO, CeO_2, CdS, and ZnS. TiO_2 is particularly favored for its stability, low cost, non-toxicity, and high photocatalytic activity.[10] TiO_2's efficiency is influenced by several factors, including its crystal phase, surface area, particle size, band gap energy, and surface hydroxylation.[11] However, TiO_2 is primarily UV-active due to its wide band gap (3.2 eV), limiting its efficiency under natural sunlight, where UV light constitutes less than 5% of the spectrum.[12] To address this limitation, strategies have been explored to extend TiO_2's photo-response into the visible light region (~45% of sunlight). Modifications include doping with metal or non-metal ions, forming heterojunction composites, and sensitization with dyes.[13] Among these, dye sensitization stands out for its simplicity, affordability, and efficiency in enhancing visible-light absorption.[14] Sensitizer dyes absorb photons in the visible range and transfer excited electrons to the conduction band of TiO_2, initiating photocatalytic reactions.[15] While synthetic dyes such as eosin-Y, rhodamine-B, methylene blue, and ruthenium complexes have been extensively used for sensitization, they often pose environmental hazards, involve complex synthesis, and lack long-term stability. In contrast, natural dyes-derived from eco-friendly sources such as fruits, leaves, and flowers-offer a safer, renewable, and biodegradable alternative.[16] Plant-based pigments such as anthocyanins and chlorophyll, commonly found in red water lily and water hyacinth respectively, are gaining attention for their strong absorption in the visible spectrum, ease of extraction, and environmental sustainability.[17,18]

Previous studies have reported a wide variety of visible-light-active photocatalysts for pollutant degradation, including dye-sensitized TiO_2, doped TiO_2, and heterojunction-based systems.[19] For example, eosin-Y-sensitized TiO_2 has been shown to achieve over 85% methylene blue degradation under visible light, while metal-doped TiO_2 systems often reach comparable efficiencies but suffer from long-term instability due to dopant leaching.[20] Similarly, heterojunctions such as TiO_2–CdS and TiO_2–ZnO composites extend visible-light activity but raise concerns of toxicity and cost.[21] In contrast, natural dye-sensitized systems have reported moderate to high degradation efficiencies (60–80%) with better eco-compatibility and lower fabrication costs.[22] However, stability remains a critical challenge, as many natural dyes undergo photobleaching. In this context, the present work focuses on anthocyanin and chlorophyll as natural sensitizers for TiO_2. Compared to synthetic dye-sensitized or doped TiO_2 systems, our approach emphasizes sustainability, material abundance, and reusability. Importantly, by systematically comparing photocatalytic efficiency, stability over multiple reuse cycles, and mechanistic aspects such as electron transfer from dye molecules to TiO_2, this study aims to position natural dye-sensitized TiO_2 within the broader field of visible-light photocatalysis.

The research aims to enhance the photocatalytic performance of TiO_2 nanoparticles (NPs) when exposed to visible light. The TiO_2 NPs were then sensitized using natural anthocyanin extract from red water lily and chlorophyll extract from water hyacinth. This approach aims to bridge the gap between green chemistry and practical wastewater treatment by leveraging nature-inspired solutions for the degradation of harmful organic pollutants under visible light illumination.

2. Methods and materials

2.1 Materials

As the photocatalyst, anatase-phase TiO_2 nanoparticles (titanium(IV) oxide, AEROXIDE® P25, Tokyo Chemical Industry Co., Ltd, Japan; 99% purity) were employed. The material was chosen for photocatalytic applications because of its small primary particle size (average of 21 nm) and high specific surface area (35–65 $m^2\ g^{-1}$, BET method). Ethanol and methanol were used as solvents to extract natural dyes from locally collected red water lily (*Nymphaea rubra*) and water hyacinth (*Eichhornia crassipes*), which were then rinsed with deionized water. Glassware was pre-treated with 10% nitric acid and thoroughly rinsed, and deionized water was used throughout the process to guarantee purity. As needed, HCl and NaOH were used to raise the pH of the solutions. Methylene blue (MB) was selected as the model pollutant, and all chemicals were used as received without further purification.

2.2 Preparation of natural dye extracts

Red water lily flowers and water hyacinth leaves serve as the sources for anthocyanin and chlorophyll dyes, respectively, with their extraction being performed following previously reported and well-established procedures,[23,24] which are known to provide high-purity pigments suitable for photocatalytic and photoelectrochemical applications. The extraction solvents and conditions were optimized to minimize degradation and ensure pigment stability. However, we acknowledge that the exact yield and purity of the extracted dyes were not quantitatively determined in this work.

To improve pigment stability, 100 mL of an ethanol–water solution (70 : 30 v/v) acidified with 0.1% HCl was combined with 10 g of dried and manually crushed red water lily petals. To optimize dye extraction, the mixture was heated to 100 °C for 5 min in a water bath and then left to stand at room temperature for 24 h in a dark environment. Following filtration through Whatman No. 1 paper, a rotary evaporator was used to concentrate the filtrate for 3 h at 40 °C. The resultant extract was kept in amber bottles at 4 °C until it was needed again.

10 g of fresh green water hyacinth leaves (midribs removed) were chopped and mixed with 100 mL of 90% aqueous acetone using a magnetic stirrer in order to extract the chlorophyll. To stop pigment oxidation, the slurry was left in the dark at 4 °C for 2 h. After that, it was centrifuged for 20 min at 3000 rpm. A rotary evaporator was used to concentrate the resultant solution at 40 °C for 3 h after the supernatant had been filtered through filter paper. Until it was used, the chlorophyll extract was kept at 4 °C in a tightly sealed, dark glass container. Finally, the absorption spectra were analyzed using a UV-Vis spectrophotometer.

2.3 Sensitization of TiO_2 with natural dyes

To sensitize TiO_2 nanoparticles, the method of Buddee *et al.*[25] was followed with slight modification. A total of 40 mL of concentrated dye extract was mixed with 0.4 g of TiO_2 in glass beakers and magnetically stirred for 20 h. After sensitization, the mixture was centrifuged at 3000 rpm for 10 min. The samples were then rinsed with the original solvent to remove unbound dye. Following washing, the samples were oven-dried at 70 °C for 20 h. The dried material was manually ground using an agate mortar to maintain fine consistency and prevent agglomeration.

2.4 Characterization method

The structural, optical, and thermal properties of TiO_2 nanoparticles before and after sensitization with chlorophyll and anthocyanin dyes were characterized using multiple techniques. FTIR spectroscopy (500–4000 cm^{-1}) identified functional groups and dye- TiO_2 interactions. UV-Vis spectroscopy assessed optical properties and bandgap energy. SEM examined surface morphology, particle size, and agglomeration, while EDX confirmed elemental composition. XRD analysis verified the anatase crystalline phase and calculated crystallite size using the Scherrer equation. TGA evaluated thermal stability, tracking weight loss from moisture, dye degradation, and material decomposition. Together, these analyses confirmed the suitability of dye-sensitized TiO_2 for photocatalytic wastewater treatment.

2.5 Test of photocatalytic activity

To evaluate the photocatalytic performance of dye-sensitized TiO_2 nanoparticles, MB dye degradation under visible light was studied following ISO 10678 and methods in ref. 26 with slight modification. The goal was to confirm that photocatalytic activity resulted solely from visible light absorption, excluding UV interference. Experiments were carried out in 250 mL glass beakers with 100 mL of MB solution, prepared with predetermined catalyst doses, dye concentrations, and pH levels. Before irradiation, the solution was stirred at 450 rpm in the dark for 15 min to establish adsorption–desorption equilibrium, followed by 2 h of visible light exposure using a 14 W blue LED lamp (457 nm). The setup was enclosed in aluminum foil to prevent external light interference. For sensitization, 0.5 mg of each dye-sensitized catalyst (derived from red water lily and water hyacinth) was used with 100 mL of MB solution. Samples (2.5 mL) were collected every 15 min, filtered with a 0.22 μm nylon syringe filter, and analyzed for dye concentration and degradation efficiency. The effects of operational parameters-including initial pH, catalyst dose, and dye concentration-were studied by altering one variable at a time. Control experiments investigated the roles of photolysis, adsorption, and sensitization. In photocatalytic studies, the percentage of decolorization is generally determined using the following mathematical expression:[17]

$$\%\text{Decolorization} = \left(\frac{C_0 - C_t}{C_0}\right) \times 100$$

where C_0 is the initial concentration of the dye solution and C_t is the concentration of the dye solution at a particular time for the analyzed sample.

3. Result and discussion

3.1 Characterization of photocatalyst

3.1.1 FT-IR spectra analysis. Fig. 1 displays the FT-IR spectra of pure TiO_2, pure chlorophyll (Chl), pure anthocyanin (Antho), and the corresponding sensitized TiO_2 nanocomposites (Chl-Sen TiO_2 and Antho-Sen TiO_2). A broad band near 3400 cm^{-1} in the pure TiO_2 spectrum is caused by O–H stretching vibrations of surface hydroxyl groups or physisorbed water molecules,[27] while a band around 1630 cm^{-1} is caused by H–O–H bending vibrations.[28] The anatase phase of TiO_2 is confirmed by the strong absorption below 800 cm^{-1}, especially around 700 cm^{-1}, which is ascribed to Ti–O–Ti lattice stretching.[29]

Characteristic peaks for pure chlorophyll were observed at approximately 1220 cm^{-1} (C–O stretching), 1730 cm^{-1} (C=O stretching of ester or carboxylic acid groups), and 2920 cm^{-1} (C–H stretching of aliphatic chains).[30] Likewise, significant absorptions were seen in pure anthocyanin at approximately 3320 cm^{-1} (O–H stretching), 1640 cm^{-1} (C=C stretching of aromatic rings), and 1050 cm^{-1} (C–O–C stretching of ether groups).[31] Successful dye adsorption on the TiO_2 surface was confirmed by the appearance of new functional bands and the intensification of preexisting ones in the Chl-Sen TiO_2 and Antho-Sen TiO_2 spectra upon sensitization. Additional peaks around 2920 cm^{-1} and 1720 cm^{-1} were seen for Chl-Sen TiO_2, suggesting the presence of the carbonyl and aliphatic groups of chlorophyll. Polyhydroxylated anthocyanins interact with TiO_2 through hydrogen bonding or chelation, as evidenced by the broad O–H stretching around 3350 cm^{-1} and the distinct peaks at 1635 and 1410 cm^{-1} that correspond to aromatic C=C and phenolic C–O vibrations in Antho-Sen TiO_2.[32] The decrease in

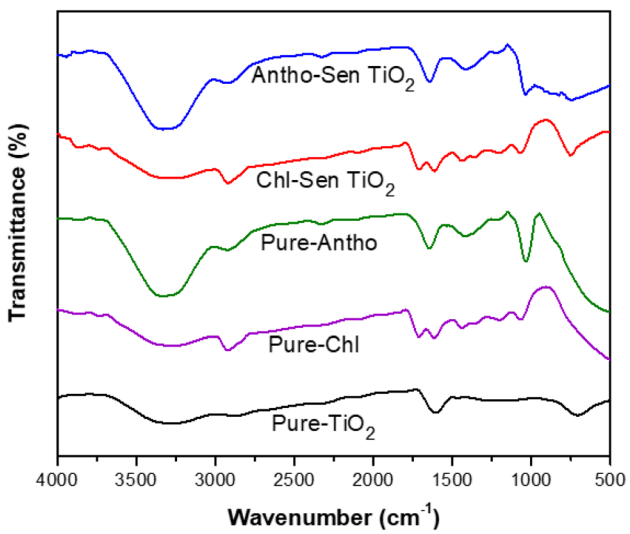

Fig. 1 FTIR spectra of Pristine TiO_2, Antho-Sen TiO_2 and Chl-Sen TiO_2.

Ti–O stretching intensity when compared to pure TiO_2 indicates that organic molecules are covering the surface. Together, these spectral changes show how natural dyes can be effectively anchored by hydroxyl and carbonyl functionalities, creating potent dye–semiconductor interactions. By facilitating charge transfer in the presence of visible light, this bonding confirms that anthocyanin and chlorophyll sensitization both considerably alter the surface chemistry of TiO_2 to increase its visible-light photocatalytic activity.

3.1.2 UV-visible spectra analysis. UV-Visible spectroscopy was used to examine the optical properties of bare TiO_2 nanoparticles and those sensitized with natural chlorophyll and anthocyanin dyes, as shown in Fig. 2. The unsensitized TiO_2 nanoparticles exhibited a strong absorption band in the UV region, typically below 400 nm, corresponding to its wide band gap (~3.2 eV), which limits its photoactivity under visible light conditions.[33] Upon sensitization with chlorophyll, TiO_2 showed enhanced absorption in the visible region, with distinct peaks observed around 420–450 nm and 660–680 nm. The $\pi \rightarrow \pi^*$ transitions in the conjugated porphyrin ring of chlorophyll are responsible for these absorption characteristics.[34] When exposed to visible light, delocalized π-electrons in the aromatic structure are excited to higher-energy π orbitals. Visible-light photocatalysis is made possible by this excitation, which lowers the effective band gap and permits electron injection from the excited dye molecules into the conduction band of TiO_2. Improved visible light-driven photocatalytic activity is made possible by this spectral shift, which indicates efficient electron excitation and transfer from the dye to the TiO_2 conduction band.

Similarly, anthocyanin-sensitized TiO_2 displayed broadened absorption bands between 500 and 550 nm, characteristic of the anthocyanin pigments. Similar functions are performed by the $\pi \rightarrow \pi^*$ transitions in the conjugated aromatic rings of anthocyanins, which are aided by hydroxyl substituents, in capturing visible photons and encouraging charge transfer to TiO_2.[35] Factors such as pH, anthocyanidin structure, and surface interaction with TiO_2 influence these optical properties.[36] The extended absorption profile suggests successful dye loading and implies a narrowed effective bandgap due to the formation of a dye–semiconductor charge transfer complex. These findings confirm that natural dye sensitization significantly extends TiO_2's optical response into the visible range, making it a promising strategy for solar-driven photocatalytic applications.

3.1.3 XRD analysis. XRD analysis was conducted to investigate the crystalline structure and phase composition of bare TiO_2 nanoparticles, along with those sensitized using natural dyes such as chlorophyll and anthocyanin. The measurements were performed over a 2θ range of 10° to 80° using Cu Kα radiation (λ = 1.5406 Å) at 40 kV and 50 mA. Crystallite sizes were estimated using the Scherrer equation, focusing on the most intense diffraction peak. The diffraction pattern of TiO_2 revealed prominent peaks at 2θ values of 25.27°, 37.96°, 48.05°, 54.17°, 62.78°, and 69.48°, corresponding to the (101), (004), (200), (105), (211), and (116) planes of the anatase phase, consistent with the standard JCPDS card no. 84-1286. Additional peaks at 27.39° and 75.12° matched the (110) and (215) planes of rutile TiO_2, according to JCPDS no. 88-1175. These results confirm that the TiO_2 samples contain both anatase and rutile phases, with anatase being predominant (Fig. 3). The average crystallite size for the (101) anatase peak was approximately 229 Å, indicating nanocrystalline nature.

The diffraction patterns of chlorophyll- and anthocyanin-sensitized TiO_2 (Chl/TiO_2 and Antho/TiO_2) showed no shift in peak positions or emergence of new phases, indicating that dye sensitization did not alter the crystal structure of TiO_2. The crystallite size for the (101) peak in Chl/TiO_2 remained around 230 Å, similar to the bare sample. In the case of Antho/TiO_2, a slightly smaller crystallite size of approximately 225 Å was

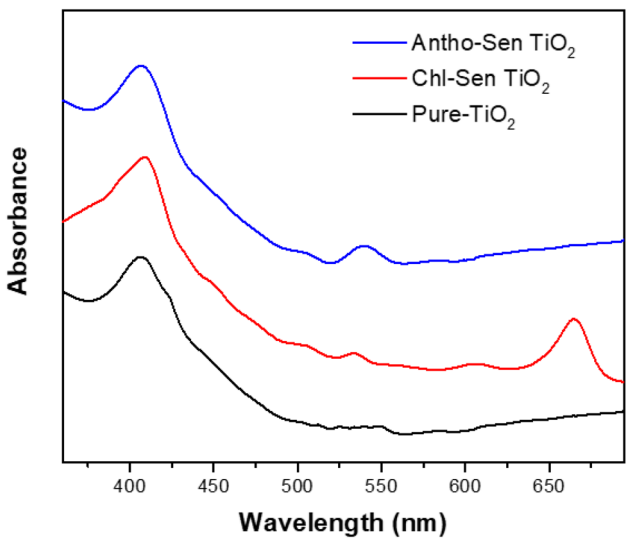

Fig. 2 UV-Vis absorbance spectra of (a) pure TiO_2, (b) chlorophyll-sensitized TiO_2, and (c) anthocyanin-sensitized TiO_2, showing distinct absorption peaks.

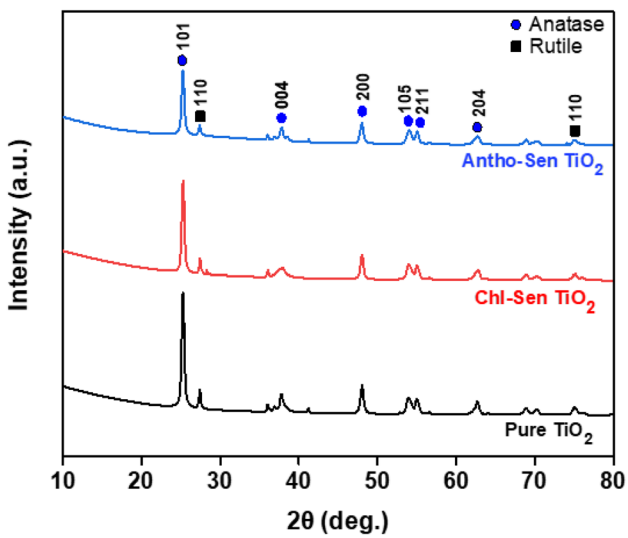

Fig. 3 XRD spectra of Pristine TiO_2, Antho-Sen TiO_2 and Chl-Sen TiO_2.

observed, possibly due to dye-induced surface strain or inhibited crystal growth. Minor variations in peak intensity may reflect surface adsorption of dye molecules, rather than structural changes.[37] Overall, the results confirm the structural integrity of TiO_2 following natural dye sensitization.

3.1.4 SEM image and EDX spectrum analysis. The surface morphology and elemental composition of bare TiO_2 and dye-sensitized TiO_2 nanoparticles were investigated using SEM coupled with EDX spectroscopy. The SEM image of bare TiO_2 (Fig. 4a) shows relatively uniform, spherical nanoparticles with slight agglomeration, forming compact nanoclusters. These features are typical of unmodified TiO_2 and indicate high crystallinity and purity. The corresponding EDX spectrum confirms the presence of Ti and O as the dominant elements, without detectable impurities, verifying the material's compositional integrity.

Upon sensitization with chlorophyll dye extracted (Fig. 4b), the SEM micrograph reveals a rougher and denser surface morphology compared to pure TiO_2. The TiO_2 particles appear more aggregated, and their spherical shape becomes less

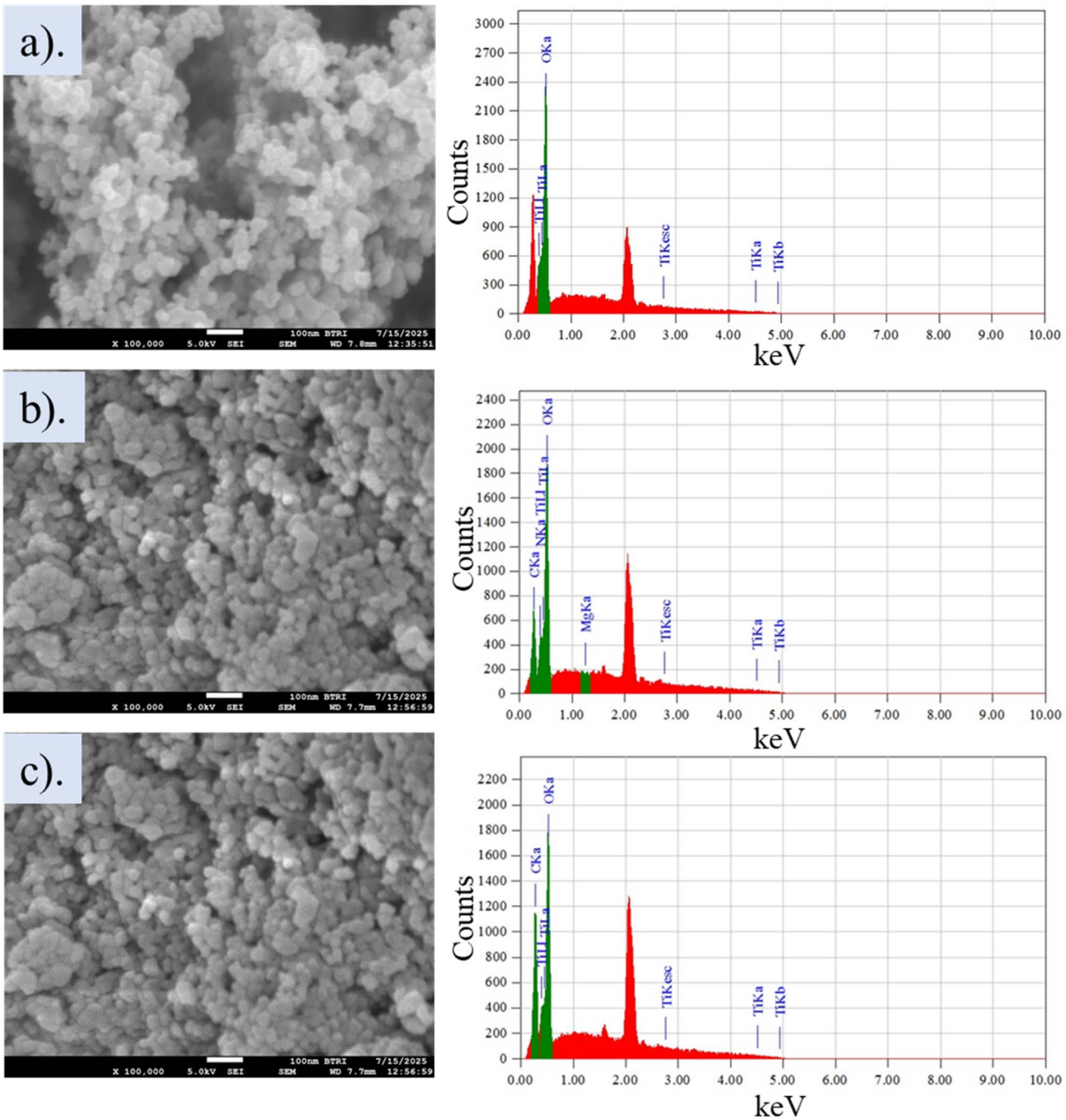

Fig. 4 SEM image and corresponding EDX spectrum of (a) Pure TiO_2, (b) Chlorophyll-Sensitized TiO_2, (c) Anthocyanin-Sensitized TiO_2.

distinct, suggesting the formation of a thin chlorophyll coating layer. This morphological modification can be attributed to the adsorption of chlorophyll molecules, which contain conjugated porphyrin rings and long hydrocarbon tails that tend to cluster on the TiO_2 surface through π–π* interactions and hydrogen bonding. The EDX spectrum further supports this, displaying additional peaks for C, N, and Mg-elements characteristic of the porphyrin core and organic structure of chlorophyll. The detection of Mg, in particular, confirms the incorporation of chlorophyll molecules onto the TiO_2 surface.

Similarly, anthocyanin-sensitized TiO_2 nanoparticles (Fig. 4c) have an even smaller and less uniform surface morphology than both bare and chlorophyll sensitize samples. The nanoparticles, which exhibit mild porosity and surface roughness, suggest successful dye-attachment and the synergistic action of polyhydroxylated anthocyanin molecules with the hydroxyl groups of the TiO_2 surface. They are believed to be associated with the hydrogen bonding and partial chelation between carbonyl/hydroxyl groups in anthocyanin and Ti atoms on the surface of TiO_2 particles. EDX data indicated obvious C and O peaks along with the weak N signal, consistent with anthocyanin molecular composition, and verified uniformed distribution of organics species on the surface of TiO_2. Overall, the SEM and EDX analyses show that both chlorophyll and anthocyanin were successfully adsorbed onto TiO_2 nanoparticles without changing their primary crystalline morphology. They also show that dye loading was successful and that the surface coverage was uniform.

3.1.5 TGA analysis. TGA assessed thermal stability and organic content of chlorophyll- and anthocyanin-sensitized TiO_2 compared to commercial TiO_2. The TGA curve for pure TiO_2 nanoparticles showed negligible weight loss (typically <1%) over the temperature range of 30–800 °C, indicating their excellent thermal stability and absence of volatile organic matter, as expected for commercially available, high-purity TiO_2.[17]

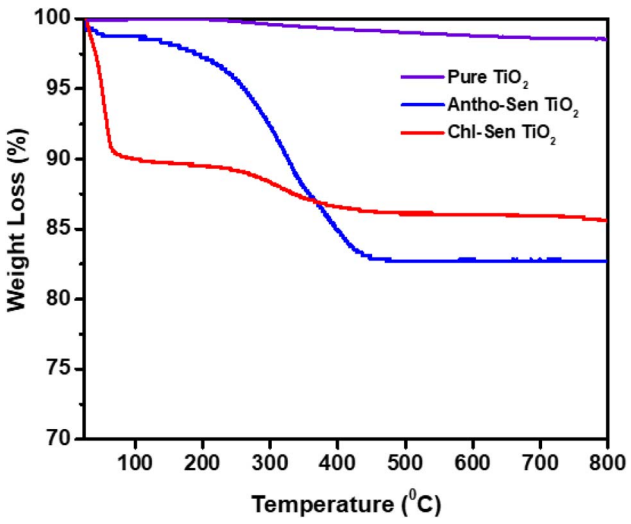

Fig. 5 TGA curves of dye-sensitized TiO_2 showing their thermal stability.

The chlorophyll-sensitized TiO_2 nanoparticles exhibited a two-step weight loss pattern, as shown in Fig. 5. At temperatures below 120 °C, a slight weight reduction of about 2–3% occurs, likely due to the evaporation of physically adsorbed moisture. A significant drop in weight, approximately 12–14%, occurred as the temperature increased from 200 to 500 °C which is associated with the decomposition of the chlorophyll dye molecules adsorbed on the TiO_2 surface. This thermal behavior confirms the successful incorporation of organic dye on the TiO_2 nanoparticles.

Similarly, the anthocyanin-sensitized TiO_2 sample showed a slightly higher total weight loss approximately 15–16% in the same temperature range, consistent with the higher molecular content and greater adsorption of anthocyanin on the nanoparticle surface. The initial mass loss below 150 °C is again linked to moisture, while the major degradation phase between 200 and 500 °C corresponds to the breakdown of anthocyanin compounds.[38] Beyond 500 °C, the weight remained relatively constant, indicating complete decomposition of the organic matter. TGA confirms dye loading on TiO_2 and shows both dyes remain stable below 200 °C, suitable for ambient applications.

3.2 Photodegradation performance of methylene blue dye

3.2.1 Effect of natural dyes sensitization on TiO_2. The photocatalytic efficiency of TiO_2 under visible light was significantly enhanced by sensitization with natural plant dyes-chlorophyll and anthocyanin (Fig. 6a). These dyes act as photosensitizers, enabling TiO_2 to harness visible light by injecting photoexcited electrons into its conduction band. To investigate the effect of dye concentration, different volumes (10, 20, 30, and 40 mL) of each dye were used for sensitization. The photocatalytic performance was then evaluated by monitoring the degradation of a model dye pollutant under visible light for 120 min. The degradation efficiency increased with increasing dye volume. Chlorophyll-sensitized TiO_2 achieved degradation rates of 44%, 46%, 50%, and 66% for 10, 20, 30, and 40 mL, respectively. Anthocyanin-sensitized TiO_2 outperformed its chlorophyll counterpart with degradation efficiencies of 56%, 59%, 60%, and 75% for the corresponding volumes. The enhancement is attributed to better light harvesting and increased generation of photo-induced electrons at higher dye concentrations.[39]

The mechanism involves visible light absorption by the dye molecules, followed by electron injection into the TiO_2 conduction band. These electrons participate in generating reactive oxygen species (ROS) such as hydroxyl radicals ($^{\bullet}OH$) and superoxide anions ($O_2^{\bullet-}$), which drive pollutant degradation.[40] Among the two dyes, anthocyanin demonstrated superior photocatalytic enhancement, likely due to its extended absorption range and strong interaction with TiO_2.[41] Its flavonoid structure with multiple hydroxyl groups enhances electron transfer and dye binding, making it a more effective natural sensitizer than chlorophyll. These results confirm the promise of eco-friendly, cost-effective dye sensitization for visible-light-driven photocatalysis.

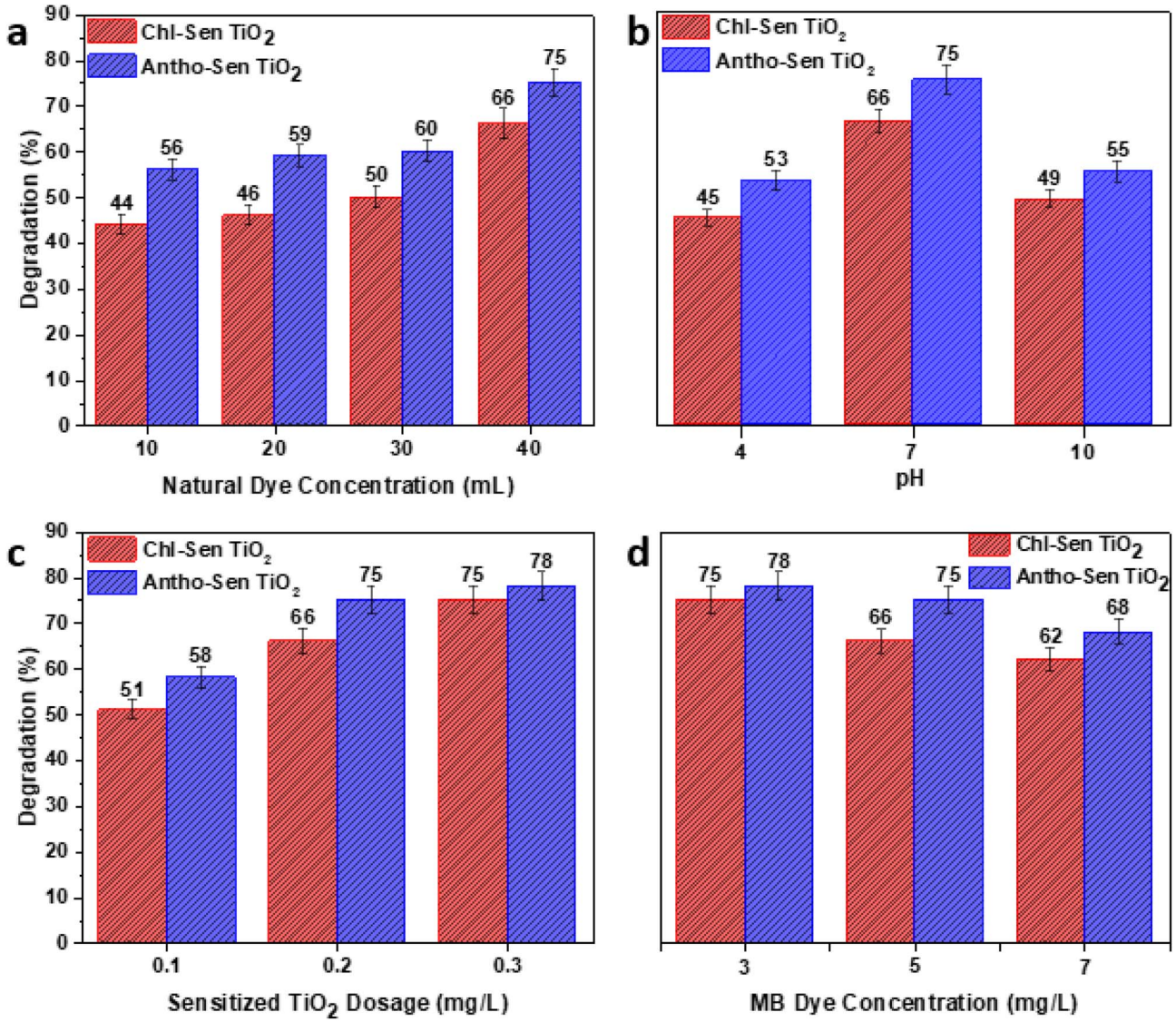

Fig. 6 Effect of (a) natural dye type, (b) pH during sensitization, (c) TiO_2 dosage, and (d) initial MB concentration on the photocatalytic degradation efficiency of dye-sensitized TiO_2 under visible light irradiation.

3.2.2 Effect of pH on photocatalytic efficiency. The photocatalytic activity of dye-sensitized TiO_2 is significantly influenced by the pH of the solution, as it alters both the surface charge of TiO_2 and the stability of the dye molecules, thus impacting pollutant degradation efficiency. To assess this effect, photocatalytic experiments were conducted at pH 4, 7, and 10 using chlorophyll- and anthocyanin-sensitized TiO_2.

Both systems demonstrated their highest degradation performance at neutral pH, with chlorophyll-sensitized TiO_2 achieving 66% degradation and anthocyanin-sensitized TiO_2 reaching 75%, as shown in Fig. 6b. In contrast, degradation efficiencies were lower at pH 4–45% for chlorophyll and 53% for anthocyanin- and decreased again at pH 10 to 49% and 55%, respectively. This trend suggests that neutral pH conditions provide the most favorable environment for photocatalytic reactions.[42] At pH 7, TiO_2's surface is near its point of zero charge (PZC), promoting effective dye adsorption and interaction, which enhances the generation of reactive oxygen species (ROS) like hydroxyl radicals. These ROS are crucial in degrading pollutants. In acidic conditions, the positively charged TiO_2 surface may repel cationic dye molecules, reducing adsorption. Although basic media offer abundant hydroxide ions, excessive alkalinity can destabilize dye molecules or hinder their interaction with TiO_2.[43] The zeta potential curve (Fig. 7) shows that TiO_2 has a positive surface charge in the acidic region. As pH rises, this charge gradually changes to negative values, with the point of zero charge (PZC) being around pH 6.5–6.8. The electrostatic interactions between TiO_2 and methylene blue (MB) molecules are directly affected by this reversal of surface charge. The predominant MB species in solution remain cationic at pH values above 3.8 because the pKa of MB is roughly 3.8.[44,45] Additionally, according to reports by S. Hemdan, MB changes color in response to structural changes.[46] This is because it changes from a diprotonated cationic form

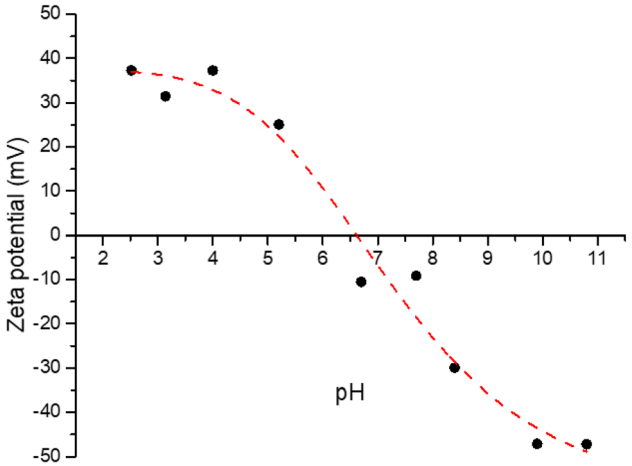

Fig. 7 TiO_2 zeta potential as a function of pH, with a zero charge point close to pH 7, exhibiting a positive charge in acidic and a negative charge in basic conditions.

(pH 2–4) to a monoprotonated cationic form (pH 5–7) and then to a quinoidal cationic form (pH ≥ 8), which reflects its changing electronic configuration with pH. So, the MB molecules still carry the positive charge and bind through an electrostatic attraction with TiO_2 nanoparticles, even if the pH is above 7. However, the excess pH (pH 10) makes the MB charge negative, that makes unfavorable to attach with TiO_2 nanoparticle, resulting in low degradation efficiency. During sensitization, these structural alterations also affect the dynamics of electron transfer and light absorption. Near-neutral pH conditions offer the best balance between dye stability, adsorption, and surface charge compatibility, resulting in the highest photocatalytic efficiency for dye-sensitized TiO_2 systems, according to the combined analysis of zeta potential behavior and photocatalytic performance.

3.2.3 Effect of dye-sensitized TiO_2 dosage. The dosage of dye-sensitized TiO_2 is a key factor influencing photocatalytic degradation efficiency. In this study, chlorophyll- and anthocyanin-sensitized TiO_2 nanoparticles were tested at concentrations of 0.1, 0.2, and 0.3 g L^{-1} under neutral pH conditions to evaluate their performance under visible light. Results showed that increasing the catalyst dosage enhanced the degradation efficiency in both systems, as shown in Fig. 6c. This improvement is attributed to the higher number of active sites available for dye adsorption and the generation of ROS, which are essential for photocatalytic breakdown of pollutants.[47] Higher photocatalyst concentrations increase the available surface area and light absorption, thereby promoting photocatalytic reactions.[48] Moreover, more TiO_2 particles enhance dye adsorption on the catalyst surface, facilitating efficient electron transfer between the dye and TiO_2-an essential mechanism in dye-sensitized systems.[49] At the highest dosage of 0.3 g L^{-1}, both systems achieved their peak degradation rates, exceeding 75%. However, considering the economic feasibility, the optimum catalyst dosage was selected as 0.2 g L^{-1}, as it achieved sufficiently high degradation efficiencies of 66% for chlorophyll-sensitized TiO_2 and 75% for anthocyanin-sensitized TiO_2. Increasing the catalyst concentration to 0.3 g L^{-1} resulted in only a 9% increase for chlorophyll-sensitized TiO_2 and a 4% increase for anthocyanin-sensitized TiO_2 in overall efficiency.

3.2.4 Effect of initial MB dye concentration. The initial concentration of MB dye is a critical parameter affecting photocatalytic degradation efficiency. In this study, the influence of different MB concentrations- 3 mg L^{-1}, 5 mg L^{-1}, and 7 mg L^{-1} on the photocatalytic performance of chlorophyll- and anthocyanin-sensitized TiO_2 was examined. Experiments were conducted using a fixed catalyst dosage of 0.2 g L^{-1} at an initial pH of 7. As shown in Fig. 6d, the degradation efficiency of both dye-sensitized systems decreased with increasing MB concentration. At 3 mg L^{-1}, chlorophyll-sensitized TiO_2 achieved 75% degradation, while anthocyanin-sensitized TiO_2 reached 78%. However, at 5 mg L^{-1}, degradation dropped to 66% and 75% for chlorophyll and anthocyanin systems, respectively. Further increasing the MB concentration to 7 mg L^{-1} led to a decline in performance-62% for chlorophyll- and 68% for anthocyanin-sensitized TiO_2.

This inverse relationship can be explained by reduced light penetration and limited generation of hydroxyl ($^{\bullet}OH$) radicals at higher dye concentrations.[50] Excessive MB absorbs incident light, preventing sufficient activation of the photocatalyst. Moreover, increased dye concentration generates more intermediate byproducts that compete for available $^{\bullet}OH$ radicals, thereby hindering overall degradation efficiency.[51] Although the highest degradation occurred at 3 mg L^{-1}, 5 mg L^{-1} was selected as the optimum concentration for further studies, as it represents a more realistic pollutant load in typical wastewater. This balance between efficient degradation and practical applicability aligns with prior findings, where moderate pollutant levels yielded optimal photocatalytic performance.[52]

Below presents a critical comparison of this work with previously reported materials in terms of degradation efficiency and stability. It highlights that natural pigment-sensitized TiO_2, particularly those using anthocyanin and chlorophyll, demonstrates markedly enhanced photocatalytic efficiency and stability under visible light compared to bare TiO_2 (Table 1).

3.3 Reusability study

The long-term usability and stability of photocatalysts are essential for their deployment in real wastewater treatment systems. To assess this, the reusability of chlorophyll-sensitized TiO_2 and anthocyanin-sensitized TiO_2 was examined over five consecutive photocatalytic degradation cycles under visible light irradiation, as shown in Fig. 8.

After each cycle, the photocatalysts were recovered by centrifugation, washed thoroughly with distilled water and ethanol to remove surface-adsorbed intermediates or residual dyes, and then dried before reuse. As illustrated in Figure, the anthocyanin-sensitized TiO_2 exhibited higher and more stable degradation efficiency across all cycles compared to its chlorophyll counterpart. In the first cycle, Antho-sen TiO_2 achieved 75% degradation, followed by 72%, 68%, 64%, and 61% in subsequent cycles. Meanwhile, Chl-sen TiO_2 began with 66%

Table 1 Comparison of photocatalytic performance of TiO_2 and natural dye-sensitized TiO_2 systems under visible light

Materials	Sensitizer	Conditions	Degradation efficiency	Stability	Ref.
TiO_2 (bare)	None	Visible light (457 nm), pH 7, 0.2 g L^{-1} catalyst, 5 mg L^{-1} MB^{-1}	38 ± 2	—	This work
TiO_2	Chlorophyll (*Eichhornia crassipes*)	Visible light (457 nm), pH 7, 0.2 g L^{-1} catalyst, 5 mg L^{-1} MB^{-1}	66 ± 3	82% retained activity after 5 cycle	
TiO_2	Anthocyanin (*Nymphaea rubra*)	Visible light (457 nm), pH 7, 0.2 g L^{-1} catalyst, 5 mg L^{-1} MB^{-1}	75 ± 3	83% retained activity after 5 cycle	
TiO_2	Eosin-Y (synthetic dye)	Visible light (>400 nm), 300 W Xe lamp	75 ± 2	60% retained after 3 cycles	20
TiO_2	Curcumin (natural dye)	Visible light (λ = 450 nm)	70 ± 4	75% retained after 5 cycles	21
TiO_2	Anthocyanin (*Syzygium cumini*)	Visible light (λ = 420 nm)	72 ± 3	70% retained after 4 cycles	22
TiO_2–ZnO composite	None (heterojunction)	Visible light (λ > 420 nm), 300 W Xe lamp; 0.1 g L^{-1} catalyst; 5 mg L^{-1} dye	78 ± 3	78% retained after 5 cycles	33
TiO_2 (Ag-doped)	None	Visible light (λ > 400 nm), 0.2 g L^{-1} catalyst; pH 7; 5 mg L^{-1} dye	73 ± 2	70% retained after 3 cycles	
TiO_2 (N-doped)	Nitrogen dopant	Visible light (λ > 420 nm), 300 W Xe lamp; 0.2 g L; 10 mg L^{-1} MB^{-1}; 120 min	70 ± 3	75% retained (5 cycles)	13
TiO_2/Graphene	Graphene nanosheets	Visible light (λ > 420 nm), 0.2 g L; 10 mg L^{-1} phenol; 120 min	90 ± 2	77% retained (6 cycles)	49
TiO_2/CdS	CdS quantum dots	Visible light (>420 nm), 300 W Xe lamp; 0.1 g L; 5 mg L^{-1} MB^{-1}	92 ± 2	65% retained (3 cycles)	13
TiO_2/Fe_2O_3	Iron oxide (hematite)	Visible light (>420 nm), 0.2 g L; 10 mg L^{-1} phenol; 120 min	78 ± 3	80% retained (4 cycles)	49
TiO_2	Anthocyanin (flower/leaf source)	Visible light, combined with electrocoagulation, 0.2 g L; 10 mg L^{-1} MB^{-1}; 48 min	∼64.3% in combined process in 48 min	—	53
TiO_2	Biomass pigments (chlorophyll & phycocyanin)	Visible irradiation, thin film; 0.1 g L^{-1} catalyst; 120 min	∼25.3% degradation after sensitization	—	54
TiO_2	Roselle flower (*Hibiscus sabdariffa*)	Visible light (>420 nm), 0.2 g L; pH 7; 10 mg L^{-1} MB^{-1}; 150 min	67 ± 2	75% retained (5 cycles)	55
TiO_2	Green tea extract (*Camellia sinensis*)	Visible light (λ > 420 nm), 0.1 g L; 10 mg L^{-1} CR; 120 min	72 ± 3	75% retained (4 cycles)	56
TiO_2	Spinach chlorophyll	Visible light (λ > 400 nm), 0.1 g L; 5 mg L^{-1} RhB; 100 min	74 ± 2	68% retained (5 cycles)	57

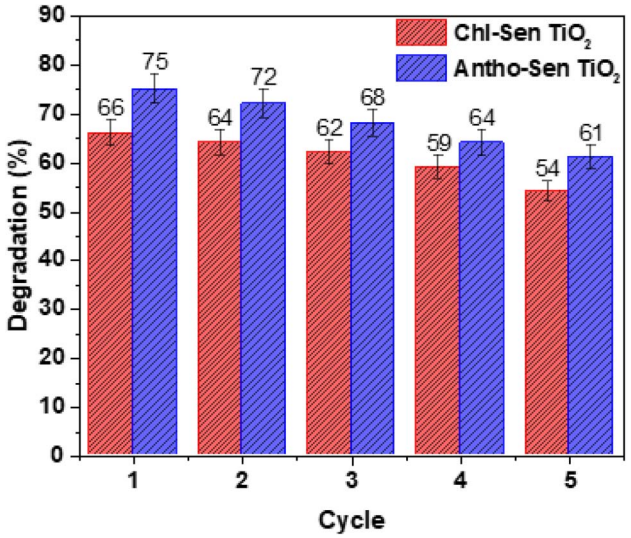

Fig. 8 Reusability of sensitized TiO_2 over five cycles, showing enhanced stability and degradation efficiency under visible light irradiation.

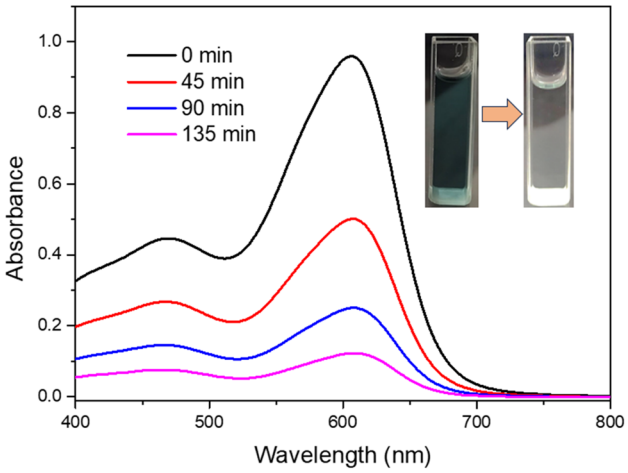

Fig. 9 The UV-Vis spectra of actual textile wastewater were obtained both before and after photocatalytic degradation. The inset confirms effective degradation under actual wastewater conditions by displaying a color shift from dark blue to almost colorless.

degradation, which gradually declined to 64%, 62%, 59%, and 54% over the five cycles.

This slight decrease in photocatalytic efficiency upon reuse may be attributed to several factors. Primarily, some loss of dye molecules from the TiO_2 surface may occur during the washing process, reducing the light absorption capacity in later cycles. Additionally, the accumulation of intermediate degradation products might block active sites or reduce surface reactivity. Other factors could include partial agglomeration of nanoparticles, structural changes during photocatalysis, or photobleaching of the dye molecules. Despite these potential issues, both photocatalysts retained a significant portion of their initial activity, with Antho-sen TiO_2 retaining over 81% and Chl-sen TiO_2 about 82% of their initial degradation efficiency by the fifth cycle. The relatively better performance of anthocyanin-sensitized TiO_2 may be due to the chemical stability of anthocyanins under visible light and their stronger interaction with the TiO_2 surface through hydroxyl or carbonyl groups. These findings highlight that natural dye-sensitized TiO_2 photocatalysts-especially those using anthocyanins-exhibit commendable reusability, making them promising candidates for sustainable and cost-effective photocatalytic wastewater treatment. Future improvements might focus on enhancing dye-TiO_2 bonding, optimizing dye extraction and loading methods, and employing surface protection strategies to further extend catalyst durability.

3.4 Stability in real wastewater conditions

Using actual wastewater gathered from an industrial textile dyeing area, photocatalytic degradation was carried out to assess the stability and practical applicability of the synthesized TiO_2 nanocatalyst. In order to eliminate suspended solids and large organic particles that might obstruct light penetration and catalyst dispersion, the wastewater was filtered through a nylon syringe filter before analysis. The degradation study was carried out using the anthocyanin sensitized TiO_2 with a catalyst dosage of 2.0 g L^{-1} and a pH of 7, which were the ideal experimental parameters determined by model pollutant experiments. The wastewater's UV-Vis absorption spectra before and after photocatalytic treatment are shown in Fig. 8. The presence of mixed dye contaminants and aromatic organics was the main cause of the first wastewater sample's wide absorption band in the visible region. The absorbance intensity gradually decreased after irradiation, suggesting that the colored pollutants were effectively degraded. The treated sample nearly turned colorless after 135 min of illumination, indicating that the chromophoric components had significantly broken down. This observation is further supported by the inset photograph, which depicts the visual change from a dark blue solution to one that is almost transparent. The stability and resilience of the TiO_2 nanocatalyst against competitive adsorption and radical scavenging effects, which are frequently found in actual effluents, are demonstrated by its consistent performance under such a complex wastewater matrix. Even in less-than-ideal, industrial wastewater environments, these results demonstrate that the synthesized TiO_2 nanocatalyst retains strong photocatalytic activity and structural integrity, indicating its potential for scalable wastewater treatment applications (Fig. 9).

3.5 Plausible mechanism of methylene blue degradation

The proposed mechanism for the photocatalytic degradation of MB dye using chlorophyll and anthocyanin sensitized TiO_2 under visible light illumination is shown schematically in Fig. 10.

When exposed to visible light, the pigment molecules (Pig) attached to the TiO_2 surface absorb photons, promoting electrons from the HOMO to the lowest LUMO, generating an excited singlet state (^{1}Pig*). Through intersystem crossing (ISC), these electrons can transition to a triplet state (^{3}Pig*), as

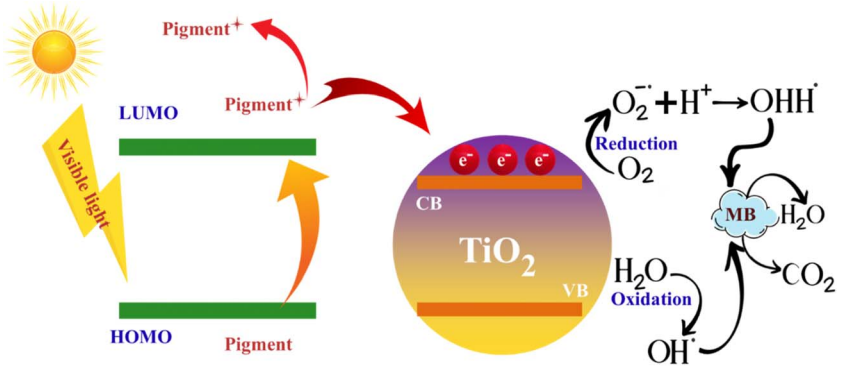

Fig. 10 Schematic representation of the dye-sensitized TiO_2 photocatalytic mechanism in visible light, demonstrating the excitation of electrons from pigment to the TiO_2 conduction band and the ensuing redox reactions that result in the degradation of MB dye.

described by Phongamwong *et al.*.[58] The photoexcited electrons from the pigment are subsequently injected into the conduction band (CB) of TiO_2, while its valence band (VB) remains unaffected under visible light exposure. This process produces pigment cation radicals (Pig^+) on the TiO_2 surface. The transferred electrons then react with adsorbed oxygen molecules (O_2) to generate superoxide radicals ($O_2^{\cdot -}$). These radicals can undergo protonation to form hydroperoxyl radicals ($H_2O^{\cdot}$), which further decompose into highly reactive hydroxyl radicals ($^{\cdot}OH$) as shown in eqn (1)–(10).[59] The positively charged MB molecules adsorbed on the negatively charged TiO_2 surface are subsequently oxidized by these reactive hydroxyl radicals, resulting in the breakdown of MB into smaller intermediates and final mineralization products. Thus, the main role of the sensitizing pigments is to activate TiO_2 indirectly under visible light, initiating the formation of reactive oxygen species such as $O_2^{\cdot -}$ and $^{\cdot}OH$, which drive the degradation of MB. The oxidized pigment radical (Pig^+) can regain its ground state by accepting an electron from an electron donor in the pigment's electron transport system,[60] enabling continuous photocatalytic cycles. Additionally, singlet oxygen ($^1O_2$) may also be produced through energy transfer during collisions between the triplet-excited chlorophyll and molecular oxygen in its ground triplet state, as expressed in eqn (9).

$$Pig \xrightarrow{h\nu \approx 457nm} {}^1Pig \quad (1)$$

$${}^1Pig \xrightarrow{ISC} {}^3Pig^* \rightarrow Pig(\text{ground state}) \quad (2)$$

$${}^1Pig^* \rightarrow Pig^* + TiO_2(e^- CB) \quad (3)$$

$${}^1Pig^* + O_2 \rightarrow Pig + {}^1O_2 \quad (4)$$

$$TiO_2(e^- CB) + O_2(\text{dissolved}) \rightarrow TiO_2(e^- CB) + O_2^{\cdot -} \quad (5)$$

$$TiO_2\ (e^- CB) + {}^1O_2(\text{dissolved}) \rightarrow TiO_2(e^- CB) + O_2^{\cdot -} \quad (6)$$

$$O_2^{\cdot -} + H_2O \rightarrow OH^- + H_2O \quad (7)$$

$$2H_2O^{\cdot} + H_2O^{\cdot} \rightarrow H_2O_2 + {}^{\cdot}OH \quad (8)$$

$$H_2O_2 \rightarrow 2{}^{\cdot}OH \quad (9)$$

$$MB + {}^{\cdot}OH, O_2^{\cdot -} \rightarrow \text{Degradation Products} \quad (10)$$

4. Importance and directions for future research

The development of natural dye-sensitized TiO_2 photocatalysts represents a significant step toward sustainable and eco-friendly wastewater treatment technologies. These materials combine the photocatalytic efficiency of TiO_2 with the light-harvesting capabilities of plant-derived dyes, enabling effective utilization of visible light-a major portion of the solar spectrum. Beyond their environmental compatibility, such systems are cost-effective and accessible, making them suitable for large-scale applications in regions with limited resources. Importantly, the use of renewable dye sources aligns with green chemistry principles, reducing dependence on synthetic, potentially hazardous photosensitizers. However, to fully harness their potential, future research should address several critical areas. First, improving dye–TiO_2 binding stability is essential to minimize leaching and enhance long-term performance. Advanced surface modification techniques, such as covalent coupling or polymer encapsulation, could provide stronger dye attachment. Second, optimizing dye extraction and purification methods will help achieve higher purity and consistent light absorption properties. Additionally, studies should explore co-sensitization strategies, combining multiple dyes to broaden the absorption spectrum and improve charge separation. Mechanistic investigations using *in situ* spectroscopic and electrochemical methods can deepen understanding of electron transfer dynamics and reactive oxygen species formation. Finally, real-world performance assessments in complex wastewater matrices, coupled with techno-economic and life-cycle analyses, will be necessary to evaluate scalability and environmental impact. Through these targeted research directions, natural dye-sensitized TiO_2 systems can evolve from promising laboratory concepts into reliable, high-performance photocatalysts for global wastewater treatment challenges.

5. Conclusions

This study demonstrates that natural plant dyes, specifically chlorophyll and anthocyanin, can effectively sensitize TiO_2 nanoparticles, enabling significant photocatalytic activity under visible light for sustainable wastewater treatment. Both dyes extended TiO_2's light absorption into the visible range, with anthocyanin-sensitized TiO_2 exhibiting superior degradation efficiencies due to its broader absorption spectrum, strong surface interaction, and enhanced electron transfer capabilities. Optimization experiments revealed that dye concentration, solution pH, catalyst dosage, and initial pollutant load critically influence photocatalytic performance. Neutral pH conditions favored maximum degradation, while excessive pollutant concentrations hindered light penetration and reduced reactive oxygen species generation. Importantly, both chlorophyll- and anthocyanin-sensitized systems retained over 80% of their initial activity after five reuse cycles, highlighting their reusability and potential for long-term application in real wastewater treatment scenarios.

The use of naturally derived sensitizers offers an eco-friendly, low-cost, and sustainable alternative to synthetic dyes or rare-metal-based modifications, aligning with green chemistry principles. By coupling abundant plant-based pigments with a widely studied and stable semiconductor such as TiO_2, this approach minimizes environmental impact while enhancing photocatalytic performance. Future research should focus on improving dye–TiO_2 binding stability, exploring co-sensitization strategies, integrating these materials into scalable reactor designs, and evaluating their performance against complex industrial effluents. Overall, bio-dye-sensitized TiO_2 nanophotocatalysts hold significant promise for next-generation, solar-driven water purification technologies.

Author contributions

Md. Abul Bashar: writing original draft; Ahmed B. M. Ibrahim: resources; Md. Kamrul Hasan, Muhammad Sarwar Hossain: methodology, validation, writing and editing, and supervision.

Conflicts of interest

The authors declare that they have no known financial or personal conflicts of interest that could have influenced the work reported in this paper.

Data availability

The data supporting the findings of this study can be obtained from the corresponding author upon request. Due to privacy concerns and other restrictions, the data are not publicly accessible.

Acknowledgements

This work was supported and funded by the Deanship of Scientific Research at Imam Mohammad Ibn Saud Islamic University (IMSIU) (grant number IMSIU-DDRSP2502).

References

1 A. P. Onyena and K. J. D. S. Sam, The blue revolution: sustainable water management for a thirsty world, *Discover Sustainability*, 2025, **6**(1), 63.
2 S. Ghosh, Sustainable technologies for removal of arsenic from water and wastewater: A comprehensive review, *J. Mol. Liq.*, 2025, **427**, 127412.
3 S. Thakur, A. Chandra, V. Kumar, and S. Bharti, Environmental pollutants: endocrine disruptors/pesticides/reactive dyes and inorganic toxic compounds metals, radionuclides, and metalloids and their impact on the ecosystem, in *Biotechnology for Environmental Sustainability*, Springer, 2025, pp. 55–100.
4 M. M. Islam, A. R. Aidid, J. N. Mohshin, H. Mondal, S. Ganguli, and A. K. Chakraborty, *A Critical Review on Textile Dye-Containing Wastewater: Ecotoxicity, Health Risks, and Remediation Strategies for Environmental Safety*, 2025, p. 100165.
5 M. Mahmoodi, E. J. E. S. Pishbin and P. Research, Ozone-based advanced oxidation processes in water treatment: Recent advances, challenges, and perspective, *Environ. Sci. Pollut. Res.*, 2025, **32**(7), 3531–3570.
6 G. Gopalakrishnan, R. B. Jeyakumar and A. Somanathan, Challenges and emerging trends in advanced oxidation technologies and integration of advanced oxidation processes with biological processes for wastewater treatment, *Sustainability*, 2023, **15**(5), 4235.
7 M. J. C. E. Kurian and Technology, *Advanced Oxidation Processes and Nanomaterials-A Review*, 2021, 2, p. 100090.
8 G. Thennarasu *et al.*, *A Comprehensive Review on the Application of Semiconductor Nanometal Oxides Photocatalyst for the Treatment of Wastewater*, 2024, pp. 1–22.
9 V. Takhar and S. J. Singh, Nanomaterials ROS: a comprehensive review for environmental applications, *Environ. Sci.:Nano*, 2025, **12**(5), 2516–2550.
10 S. J. Armaković, M. M. Savanović and S. Armaković, Titanium dioxide as the most used photocatalyst for water purification: An overview, *Catalysts*, 2022, **13**(1), 26.
11 N. S. N. Sa'aya, Exploring the effective parameters on the Photocatalytic Activity of TiO2 Nanoparticles, *S. Afr. J. Chem. Eng.*, 2025, **53**, 127–141.
12 M. M. Khan, *Photocatalysts: UV Light Active*, 2022, p. 33.
13 A. D. G. Kafadi, Recent Trends in Hydrogen Generation Using TiO2-Based Photocatalyst *via* Photocatalytic Water Splitting, *Eur. J. Inorg. Chem.*, 2025, **28**(22), 2500191.
14 A. Pallikkara and K. J. Ramakrishnan, Efficient charge collection of photoanodes and light absorption of photosensitizers: A review, *Int. J. Energy Res.*, 2020, **45**(2), 1425–1448.

15 T. Jalali, P. Arkian, M. Golshan, M. Jalali and S. Osfouri, Performance evaluation of natural native dyes as photosensitizer in dye-sensitized solar cells, *Opt. Mater.*, 2020, **110**, 110441.
16 P. Dey, Sustainable and eco-friendly natural dyes: a holistic review on sources, extraction, and application prospects, *Text. Res. J.*, 2025, **95**, 2472–2499.
17 S. Goulart, L. J. J. Nieves, A. G. Dal Bó and A. M. Bernardin, Sensitization of TiO2 nanoparticles with natural dyes extracts for photocatalytic activity under visible light, *Dyes Pigm.*, 2020, **182**, 108654.
18 M.-E. Barbinta-Patrascu, B. Bita and I. J. B. Negut, From nature to technology: Exploring the potential of plant-based materials and modified plants in biomimetics, bionics, and green innovations, *Biomimetics*, 2024, **9**(7), 390.
19 M. El Mchaouri *et al.*, *Engineering TiO2 Photocatalysts for Enhanced Visible-Light Activity in Wastewater Treatment Applications*, p. 100084, 2025.
20 Y. Li, C. Xie, S. Peng, G. Lu and S. J. Li, Eosin Y-sensitized nitrogen-doped TiO2 for efficient visible light photocatalytic hydrogen evolution, *J. Mol. Catal. A:Chem.*, 2008, **282**(1–2), 117–123.
21 H. M. Mousa, Synthesis of TiO2@ ZnO heterojunction for dye photodegradation and wastewater treatment, *J. Alloys Compd.*, 2021, **886**, 161169.
22 K. Prajapat, The evolution of organic materials for efficient dye-sensitized solar cells, *J. Photochem. Photobiol., C*, 2023, **55**, 100586.
23 M. A. Al-Alwani, A. B. Mohamad, A. A. H. Kadhum and N. A. Ludin, Effect of solvents on the extraction of natural pigments and adsorption onto TiO2 for dye-sensitized solar cell applications, *Spectrochim. Acta, Part A*, 2015, **138**, 130–137.
24 I. C. Maurya, Neetu, A. K. Gupta, P. Srivastava and L. J. Bahadur, Natural dye extracted from Saraca asoca flowers as sensitizer for TiO2-based dye-sensitized solar cell, *J. Sol. Energy Eng.*, 2016, **138**(5), 051006.
25 S. Buddee, S. Wongnawa, P. Sriprang and C. J. Sriwong, Curcumin-sensitized TiO2 for enhanced photodegradation of dyes under visible light, *J. Nanopart. Res.*, 2014, **16**(4), 2336.
26 H. Nan, H.-P. Shen, G. Wang, S.-D. Xie, G.-J. Yang and H. Lin, Studies on the optical and photoelectric properties of anthocyanin and chlorophyll as natural co-sensitizers in dye sensitized solar cell, *Opt. Mater.*, 2017, **73**, 172–178.
27 R. Zuo, Photocatalytic degradation of methylene blue using TiO2 impregnated diatomite, *Adv. Mater. Sci. Eng.*, 2014, **2014**, 1–7.
28 R. Zuo, *et al.*, Photocatalytic degradation of methylene blue using TiO2 impregnated diatomite, *Adv. Mater. Sci. Eng.*, 2014, **2014**(1), 170148.
29 H.-x. Guo, K.-l. Lin, Z.-s. Zheng, F.-b. Xiao and S.-x. Li, Sulfanilic acid-modified P25 TiO2 nanoparticles with improved photocatalytic degradation on Congo red under visible light, *Dyes Pigm.*, 2012, **92**(3), 1278–1284.
30 V. Shanmugam, S. Manoharan, A. Sharafali, S. Anandan, R. J. Murugan and B. Spectroscopy, Green grasses as light harvesters in dye sensitized solar cells, *Spectrochim. Acta, Part A*, 2015, **135**, 947–952.
31 C. Yang, Highly-efficient photocatalytic 'degradation of methylene blue by PoPD-modified TiO 2 nanocomposites due to photosensitization-synergetic effect of TiO2 with PoPD, *Sci. Rep.*, 2017, **7**(1), 3973.
32 C. Diaz-Uribe, Improvement of the photocatalytic activity of TiO2 using Colombian Caribbean species (Syzygium cumini) as natural sensitizers: Experimental and theoretical studies, *Dyes Pigm.*, 2018, **150**, 370–376.
33 N. Boudechiche, N. Morante, D. Sannino, K. Monzillo, M. Trari and Z. J. C. Sadaoui, Enhanced visible-light photocatalysis activity of TiO2/Ag nanocomposites prepared by the ultrasound-assisted sol–gel method: Characterization and degradation–mineralization of cationic and anionic dyes, *Catalysts*, 2024, **14**(12), 883.
34 T. Phongamwong, *et al.*, Novel visible-light-sensitized Chl-Mg/P25 catalysts for photocatalytic degradation of rhodamine B, *Appl. Catal., B*, 2017, **207**, 326–334.
35 G. Calogero, J.-H. Yum, A. Sinopoli, G. Di Marco, M. Grätzel and M. K. Nazeeruddin, Anthocyanins and betalains as light-harvesting pigments for dye-sensitized solar cells, *Sol. Energy*, 2012, **86**(5), 1563–1575.
36 Z. Liu, Theoretical studies of natural pigments relevant to dye-sensitized solar cells, *J. Mol. Struct.:THEOCHEM*, 2008, **862**(1–3), 44–48.
37 S. Wahyuningsih *et al.*, Alternative natural dyes in water purification: Anthocyanin as TiO2-sensitizer in rhodamin B photoelectrodegradation, in *Biophotonics Japan 2015*, 2015, 9792, 110–116: SPIE.
38 A. Zyoud, *et al.*, Alternative natural dyes in water purification: anthocyanin as TiO2-sensitizer in methyl orange photo-degradation, *Solid State Sci.*, 2011, **13**(6), 1268–1275.
39 S. Shalini, S. Prasanna, T. K. Mallick and S. J. R. Senthilarasu, Reviews, review on natural dye sensitized solar cells: Operation, materials and methods, *Renewable Sustainable Energy Rev.*, 2015, **51**, 1306–1325.
40 D. Garg, C. Majumder, S. Kumar and B. Sarkar, Removal of Direct Blue-86 dye from aqueous solution using alginate encapsulated activated carbon (PnsAC-alginate) prepared from waste peanut shell, *J. Environ. Chem. Eng.*, 2019, **7**(5), 103365.
41 D. Vásquez, F. Palominos and S. J. C. Martínez, Visible-light photocatalytic degradation of aniline blue by stainless-steel foam coated with TiO2 grafted with anthocyanins from a maqui-blackberry system, *Catalysts*, 2020, **10**(11), 1245.
42 M. N. Chong, B. Jin, C. W. Chow and C. J. W. r. Saint, Recent developments in photocatalytic water treatment technology: a review, *Water Res.*, 2010, **44**(10), 2997–3027.
43 Y. R. Smith, A. Kar and V. Subramanian, Investigation of physicochemical parameters that influence photocatalytic degradation of methyl orange over TiO2 nanotubes, *Ind. Eng. Chem. Res.*, 2009, **48**(23), 10268–10276.
44 T. K. J. P. Sen, Adsorptive removal of dye (methylene blue) organic pollutant from water by pine tree leaf biomass adsorbent, *Processes*, 2023, **11**(7), 1877–2023.

45 A. Hassan, S. K. Dutta, M. S. Hossain, M. R. Haque and M. K. Hasan, Efficient removal of cationic dye from aqueous media using alkali-treated multilayered polymer microspheres prepared *via* emulsion polymerizatio, *New J. Chem.*, 2025, **49**(4), 1377–1390.

46 S. S. Hemdan, The shift in the behavior of methylene blue toward the sensitivity of medium: Solvatochromism, solvent parameters, regression analysis and investigation of cosolvent on the acidity constants, *J. Fluoresc.*, 2023, **33**(6), 2489–2502.

47 M. Rauf and S. S. Ashraf, Fundamental principles and application of heterogeneous photocatalytic degradation of dyes in solution, *Chem. Eng. J.*, 2009, **151**(1–3), 10–18.

48 C.-C. Wang, C.-K. Lee, M.-D. Lyu and L.-C. Juang, Photocatalytic degradation of CI Basic Violet 10 using TiO2 catalysts supported by Y zeolite: An investigation of the effects of operational parameters, *Dyes Pigm.*, 2008, **76**(3), 817–824.

49 Y. Zhang, Z.-R. Tang, X. Fu and Y.-J. Xu, TiO2− graphene nanocomposites for gas-phase photocatalytic degradation of volatile aromatic pollutant: is TiO2− graphene truly different from other TiO2− carbon composite materials?, *ACS Nano*, 2010, **4**(12), 7303–7314.

50 F. Kazemi, Z. Mohamadnia, B. Kaboudin and Z. Karimi, Photodegradation of methylene blue with a titanium dioxide/polyacrylamide photocatalyst under sunlight, *J. Appl. Polym. Sci.*, 2016, **133**(19), 43386.

51 C. Xu, G. Rangaiah and X. Zhao, Photocatalytic degradation of methylene blue by titanium dioxide: experimental and modeling study, *Ind. Eng. Chem. Res.*, 2014, **53**(38), 14641–14649.

52 U. G. Akpan and B. H. Hameed, Parameters affecting the photocatalytic degradation of dyes using TiO2-based photocatalysts: a review, *J. Hazard. Mater.*, 2009, **170**(2–3), 520–529.

53 I. Kustiningsih, H. Pujiastuti, D. K. Sari, A. Rochmat and S. J. Sustainability, The addition of anthocyanin as a sensitizer for TiO2 nanotubes in a combined process of electrocoagulation and photocatalysis for methylene blue removal, *Sustainability*, 2023, **15**(21), 15384.

54 M. E. Fuziki, A. M. Tusset, O. A. dos Santos and G. G. J. R. Lenzi, Chlorophyll Sensitization of TiO2: A Mini-Review, *Reactions*, 2023, **4**(4), 766–778.

55 I. B. Narmada, Effects of Roselle (Hibiscus sabdariffa Linn.) flower extracts on various inflammatory and bone apposition biomarkers during orthodontic tooth movement: An experimental animal study, *Journal of Oral Biology and Craniofacial Research*, 2025, **15**(2), 412–420.

56 T. Zhao, C. Li, S. Wang and X. J. M. Song, Green tea (Camellia sinensis): A review of its phytochemistry, pharmacology, and toxicology, *Molecules*, 2022, **27**(12), 3909.

57 Z. Lei, Effects of nanoanatase TiO2 on photosynthesis of spinach chloroplasts under different light illumination, *Biol. Trace Elem. Res.*, 2007, **119**(1), 68–76.

58 T. Phongamwong, Novel visible-light-sensitized Chl-Mg/P25 catalysts for photocatalytic degradation of rhodamine B, *Appl. Catal., B*, 2017, **207**, 326–334.

59 P. Chowdhury, J. Moreira, H. Gomaa, A. K. J. I. Ray and E. C. Research, Visible-solar-light-driven photocatalytic degradation of phenol with dye-sensitized TiO2: parametric and kinetic study, *Ind. Eng. Chem. Res.*, 2012, **51**(12), 4523–4532.

60 C. Worathitanon, High performance visible-light responsive Chl-Cu/ZnO catalysts for photodegradation of rhodamine B, *Appl. Catal., B*, 2019, **241**, 359–366.